

Observing Application

Date: Jul 26, 2022
Proposal ID: GBT/23A-028
Legacy ID: QS360
PI: Craig Sarazin
Type: Regular
Category: Normal Galaxies, Groups, and Clusters
Total time: 35.0

Bridges of Intergalactic Gas Connecting ACT Cluster Pairs

Abstract:

The nature and location of the missing baryons in the Universe remains a major mystery. We propose MUSTANG-2/GBT observations of two close pairs of moderate-redshift galaxy clusters recently detected in the Sunyaev-Zeldovich (SZ) effect by ACT with possible intergalactic gas filaments between them. The MUSTANG-2 and ACT SZ data will be combined to model the SZ on both large and small scales. We have approved XMM-Newton X-ray observations for both of these systems, and just received the data for our first target. Both the SZ and X-ray images will allow the separation of the cluster and the filament gas. Recently, SZ and X-ray observations have been used to study the filament between the low-redshift clusters Abell 399 and 401. The combination of SZ and X-ray observations allows the density, temperature, pressure, and 3D shape of the filaments to be determined. We will search for intergalactic shocks expected to occur at the edges of filaments, and for merger features within the clusters; this can help distinguish between pre-mergers and more advanced systems. These observations will help constrain the nature of the missing baryons in the Universe.

Authors:

Name	Institution	Email	Status
Sarazin, Craig	Virginia, University of	sarazin@virginia.edu	
Hincks, Adam	Toronto, University of	adam.hincks@mail.utoronto.ca	
Mason, Brian	National Radio Astronomy Observatory	bmason@nrao.edu	
Romero, Charles	Center for Astrophysics Harvard & Smithsonian	ceromero@sas.upenn.edu	
Mroczkowski, Tony	European Southern Observatory	tony.mroczkowski@eso.org	
Moravec, Emily	Green Bank Observatory	emoravec@nrao.edu	
Dicker, Simon	Pennsylvania, University of	simon.dicker@gmail.com	
Sievers, Jonathan	McGill University	jonathan.sievers@mcgill.ca	
Devlin, Mark	Pennsylvania, University of	devlin@physics.upenn.edu	
Bhandarkar, Tanay	Pennsylvania, University of	tanayb@sas.upenn.edu	Graduating: N/A Thesis: false
Battistelli, Elia	Roma La Sapienza, UniversitÃ degli Studi di	elia.battistelli@roma1.infn.it	
Hilton, Matt	KwaZulu-Natal, University of	hiltonm@ukzn.ac.za	
Hughes, John	Rutgers, The State University of New Jersey	jph@physics.rutgers.edu	
Radiconi, Federico	Roma La Sapienza, UniversitÃ degli Studi di	federico.radiconi@roma1.infn.it	Graduating: 2022 Thesis: false

Name	Institution	Email	Status
Di Mascolo, Luca	Trieste, UniversitÃ degli Studi di	luca.dimascolo@units.it	
Orlowski-Scherer, John	Pennsylvania, University of	jorlo@sas.upenn.edu	Graduating: N/A Thesis: false
Gill, Ajay	Toronto, University of	ajay.gill@mail.utoronto.ca	Graduating: N/A Thesis: false
Vargas, Cristian	Pontificia Universidad CatÃ³lica de Chile	cvargas@astro.puc.cl	Graduating: N/A Thesis: false
Wollack, Edward	National Aeronautics and Space Administration	edward.j.wollack@nasa.gov	
Haridas, Saianeesh	Pennsylvania, University of	haridas@sas.upenn.edu	Graduating: N/A Thesis: false
Perez Sarmiento, Karen	Pennsylvania, University of	kaper@sas.upenn.edu	Graduating: 2025 Thesis: false

Principal Investigator: Craig Sarazin
 Contact: Craig Sarazin
 Telephone: 1-434-924-4903
 Email: sarazin@virginia.edu

Related Proposals:

Joint:

Not a Joint Proposal.

Observing type(s):

Continuum, OTF Mapping

GBT Resources

Name	Group	Frontend & Backend	Setup
MUSTANG2 (Shared Risk)	ACT-CL0012	Mustang 2 Mustang 2	Number of Banks: 0
MUSTANG2 (Shared Risk)	ACT-CL1512	Mustang 2 Mustang 2	Number of Banks: 0

Sources

Name	Position		Velocity		Group	
ACT-CLJ0012.8-0855-J0012.9-0857	Coordinate system	Equatorial	Convention	Redshift	ACT-CL0012	
	Equinox	J2000				
	Right Ascension	00:12:53.21	Ref. frame	CMB		
		00:00:00.0				
	Declination	-8:56:26.40	Velocity	0.345		
		00:00:00.0				
	Calibrator	No				

Name	Position		Velocity		Group	
ACT-CLJ1512.8+1418-J1512.8+1420	Coordinate system	Equatorial	Convention	Redshift	ACT-CL1512	
	Equinox	J2000				
	Right Ascension	15:12:49.25	Ref. frame	CMB		
		00:00:00.0				
	Declination	+14:19:55.20	Velocity	0.179		
		00:00:00.0				
Calibrator		No				

Sessions:

Name	Session time (hours)	Repeat	Separation	LST minimum	LST maximum	Elevation minimum
ACT-CLJ0012.8-0855	4.0	2	0 day	10:35:46	03:24:26	25
ACT-CLJ1512.8+1418	4.5	6	0 day	10:35:46	03:24:26	25

Session Constraints:

Name	Scheduling constraints	Comments
ACT-CLJ0012.8-0855	Standard MUSTANG-2 constraints	
ACT-CLJ1512.8+1418	Standard MUSTANG-2 constraints	

Session Source/Resource Pairs:

Session name	Source	Resource	Time
ACT-CLJ0012.8-0855	ACT-CLJ0012.8-0855-J0012.9-0857	MUSTANG2 (Shared Risk)	4.0 hour
ACT-CLJ1512.8+1418	ACT-CLJ1512.8+1418-J1512.8+1420	MUSTANG2 (Shared Risk)	4.5 hour

Plan of dissertation: no

Technical Justification:

Dates:

NA

Observing time:

Our goals with the MUSTANG-2/GBT images are to be able to determine accurate SZ profiles for each of the clusters in the pairs (in order to be able to remove them from the filament, or more correctly, fit them accurately along with a model for the filament), and to detect the filaments. We determine the required exposure based on the existing ACT images of the cluster pairs (Fig. 4 in the Science Justification; Hilton et al. 2021), and on the model for the filaments discussed in the Scientific Justification and in Hincks et al. (2022).

For each of the clusters, we used the ACT images to determine their total (integrated) SZ signal, Y . We used the Universal Pressure Profile A10 from Arnaud et al. (2010, A&A, 517, 92), which fits the SZ observations of clusters reasonably well (e.g., Romero et al. 2017, ApJ, 838, 86).

Of course, the detection of intercluster filaments is new territory, so that we cannot rely on established catalogs of properties. (That is why this science is particularly exciting!). We assume that the mass of the filaments in our pairs scales with the total mass of the cluster pair, taking the constant of proportionality

from the A399-401 Bridge (Hincks et al. 2022). We assume that filaments follow a correlation between total SZ signal Y and mass M, with the same slope as that for clusters (Arnaud et al. 2010) and with the normalization set by the observations of the the A399-401 Bridge (Hincks et al. 2022). This leads to a total SZ signal of $Y_{\text{filament}} = 5.14E-6 \text{ Mpc}^2$ for our first cluster pair and $2.66E-6 \text{ Mpc}^2$ for our second cluster pair. Based on the ACT SZ images, we further assume that each filament will have an area of roughly $\sim 4 \text{ (arcmin)}^2$. This translates to a surface brightness of 42 and 21 μK for the first and second pair, respectively. The sensitivities of 42 μK and 21 μK will be sufficient to detect and image the filaments over a region of ~ 100 MUSTANG-2 beams, which is about twice the expected areas of the filaments.

We will use OTF mapping with MUSTANG-2. Documented sensitivities can be found at <https://greenbankobservatory.org/science/gbt-observers/mustang-2/>. The typical mapping speed of MUSTANG-2 is 77 μK root-hour for a SNR of 1 sigma per beam for our 3.5' scan pattern. The on-source exposure times are thus $(77/42)^2 = 3.4$ hours and $(77/21)^2 = 13.5$ hours, respectively. We round the first pair up to 4 hours to avoid less efficient short sessions (see below). Also, as noted below, we double these on-source times for overhead. This leads to total MUSTANG-2 exposures of 8 hours and 27 hours, respectively. (See Table 1 in the Science Justification.)

Mapping:

We will use the standard $r=3.5'$ MUSTANG-2 daisy scan pattern. Coverage with this scan pattern is reasonably uniform, and the scale is optimum for the separation of our cluster pairs.

RFI considerations:

RFI is not a problem at 90 GHz for MUSTANG-2.

Overhead:

MUSTANG-2 requires 100% overhead (<https://greenbankobservatory.org/science/gbt-observers/mustang-2/>), which is especially true for sessions of ~ 3 hours, while efficiency improves for longer duration sessions, such as those requested for this proposal.

Joint considerations:

NA

Novel considerations:

The data reduction technique for MUSTANG-2, Minkasi, has been published in Romero et al. 2020 and Dicker et al. 2020.

The techniques for joint fitting of MUSTANG-2 data with ACT SZ data are being developed, initially for the A399-401 Bridge. They are based on our method of joint fitting of Planck and ACT data (Hincks et al. 2022). Techniques for fitting of SZ data with X-ray data have been tested and described in Hincks et al. (2022).

Pulsar considerations:

NA

LST Range Justification:

NA

BRIDGES OF INTERGALACTIC GAS CONNECTING ACT CLUSTER PAIRS

1) Introduction

About 30% of all baryonic matter in the low-redshift Universe is not inside galaxy clusters, where it is relatively easy to observe, but outside of them, particularly in the filamentary structures connecting them, in what is called the warm-hot intergalactic medium (WHIM; see, e.g., Tuominen et al. 2021). Though the existence of the WHIM, which resolves the “missing baryon” problem, has long been inferred (Fukugita et al. 1998; Cen & Ostriker 1999), it is only in recent years that observational evidence for it has been pieced together using a variety of techniques that involve either line-of-sight absorption of light from distant sources (e.g., Macquart et al. 2020; Bouma et al. 2021) or stacking/cross-correlation of SZ or X-ray images from many clusters in order to gain signal-to-noise and see the gas in aggregate (e.g., Schaan et al. 2021; Tanimura et al. 2020a, 2020b).

Mapping out missing baryons in individual systems is much more difficult since the gas is diffuse and of moderate temperature. The thermal Sunyaev-Zeldovich (SZ) effect, due to inverse Compton scattering of the cosmic microwave background (CMB) by ionized electrons in a gas, is a promising avenue for this challenging task that has recently been demonstrated, particularly with the cluster pair Abell 399-401 (Planck Collab. 2013; Bonjean et al. 2018; Hincks et al. 2022, hereafter H22).

We propose extending this ground-breaking approach for characterizing the intercluster gas to moderate redshift cluster pairs using MUSTANG-2 SZ observations.

2) An Exemplary WHIM Filament: the Abell 399–401 Bridge

The hottest and densest WHIM is likely to be found in filaments connecting clusters of galaxies. Recently, such a filament (‘the Bridge’) connecting the two low-redshift clusters Abell 399 and 401 (hereafter A399-401) has been mapped at high resolution with the SZ effect (H22). Their mean redshift is $z = 0.0727$ and they are $37'$ (3.2 Mpc) apart in the plane of the sky. The first evidence for the Bridge, however, was found with X-ray observations, first by ASCA (Fujita et al. 1996; Markevitch et al. 1998), and then by ROSAT (Fabian et al. 1997), XMM (Sakelliou & Ponman 2004) and Suzaku (Fujita et al. 2008; Akamatsu et al. 2017). Since the X-ray images show no merger features, it is believed that the clusters have never interacted (Fujita et al. 1996; Markevitch et al. 1998; Sakelliou & Ponman 2004), but the high temperature in the bridge, 6.5 keV, could be evidence that they are moving together and compressing the gas (Sakelliou & Ponman 2004; Akamatsu et al. 2017).

X-ray observations have the advantage of higher angular resolution than the SZ, and can also provide information on the gas density, temperature, and abundances. On the other hand, the amplitude of the SZ signal at a given frequency depends linearly on the gas density since it measures the integrated pressure of the gas, as parameterized by the Compton parameter $y = (\sigma_T/m_e c^2) \int P_e(r) dr$, where σ_T is the Thomson cross section and P_e is the electron pressure (see Mroczkowski et al. 2019 for a recent review). This makes the SZ more sensitive than X-rays — which go as the density square — for diffuse gas, such as that in filaments between clusters. Nonetheless, the lower angular resolution of the SZ can be a limitation, as occurred in the Planck Collaboration (2013) report of an excess SZ signal between A399 and A401 (c.f., Bonjean et al. 2018), since they could only provide a few beams on the A399-401 bridge.

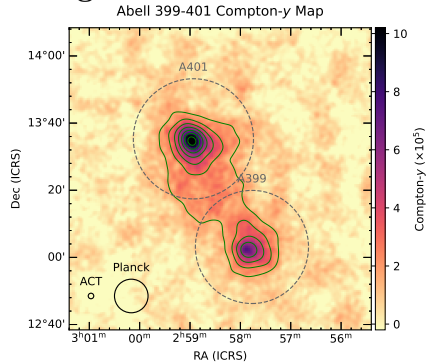


Fig. 1: Combined ACT and Planck Compton- y map of the A399-401 system, with the Bridge filament clearly visible between the clusters (H22). The beam sizes are at the lower left. Contours are 3σ to 15σ in 2σ increments. Dashed circles show r_{500} for each cluster.

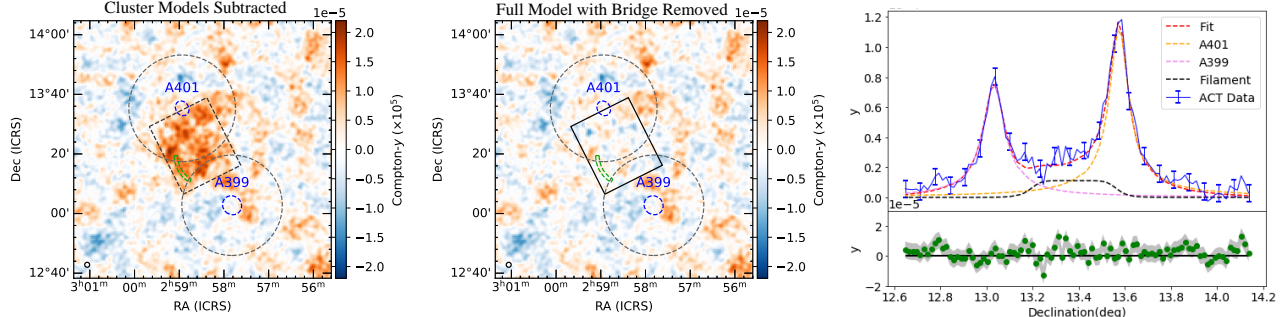


Fig. 2 (Left): Residual Planck+ACT SZ Compton- y map of A399-401, after removing just the two clusters. The Bridge excess is clear. (*Middle*): Same as Left, except that the Bridge model has now been subtracted, showing the good fit to the data. The green region is the location of a possible intergalactic shock seen in the Suzaku image (Akamatsu et al. 2017). The dashed blue ellipses show the core radii of the elliptical β -models, and r_{500} is shown in large, dashed black circles. The map's effective beam is the tiny circle in the bottom left corner. (*Right*): 1D profile of the SZ image (Fig. 1) sliced along the line connecting the centers of the two clusters, with residuals in the lower panel. The model for the Bridge filament is shown in black. All images from H22.

However, this resolution limitation was recently overcome when Planck data were augmented by maps from the Atacama Cosmology Telescope (ACT) and MUSTANG-2/GBT measurements that could much better resolve the A399-401 bridge filament and study its properties in more detail (H22). Fig. 1 shows the combined Planck+ACT SZ image of the A399-401 system. The Bridge filament between the clusters is clearly seen. To establish that this is not due to the overlapping gaseous halos of the two clusters, each of the clusters was fit with a beta model and an additional model was added for the bridge component. The residual image when only the beta models are subtracted is shown in Fig. 2 (Left). When the Bridge model is also included one obtains the residual image shown in Fig. 2 (Middle), while the Right panel shows 1D slices. The Bridge is detected to 5.5σ .

MUSTANG-2 data were used to search for small scale features in the Bridge filament. The resulting image is shown in Figure 3. Due to the limited FOV of MUSTANG-2, only A401 and the upper part of the filament are shown, and the large scale signal from the filament is resolved out.

Hincks et al. (2022) derived a number of physical properties of A399-401, which we summarize here. The width of the Bridge is ~ 1.9 Mpc, and it has an integrated Compton parameter of $Y = (4.9 \pm 1.0) \times 10^{-5}$ Mpc 2 , giving a gas mass of $(5.3 \pm 1.1) \times 10^{13} M_\odot$. The total mass of the filament is $(3.3 \pm 0.7) \times 10^{14} M_\odot$, which is about 8% of the total mass in the whole system including the clusters. The SZ image was combined with the X-ray data from Suzaku, which allows essentially all of the bulk properties of the filament to be determined. An average electron density of $(0.88 \pm 0.24) \times 10^{-4}$ cm $^{-3}$ is found for the Bridge. The combined SZ/X-ray observations imply that the filament runs substantially along the line of sight. The redshift difference between the two clusters is mainly due to infall (not cosmological expansion), and the clusters are bound.

The A399-401 system shows the value of combining SZ and X-ray observations of intergalactic filaments to determine their properties. **In the present proposal, we are trying to extend this work to moderate redshift systems that are better suited to the FOV of high resolution SZ and X-ray observations.** This requires higher spatial resolution SZ observations than are provided by either Planck or ACT. **Thus, we are proposing MUSTANG-2/GBT SZ observations.** However, in general SZ observations with a single telescope or array only cover a range of spatial scales. Thus, we will use ACT observations for the SZ at large scales, and **MUSTANG-2/GBT for the small scales**, roughly substituting Planck \rightarrow ACT, and **ACT \rightarrow**

Table 1: ACT Cluster Pairs with Possible Bridges – Properties and MUSTANG-2 Requests

ACT Cluster Pairs	$\langle z \rangle$	Separation ($'$)	Separation (kpc)	Δv_r (km/s)	M_{500c}^1 ($10^{14} M_\odot$)	M_{500c}^2 ($10^{14} M_\odot$)	t_{GBT} (hr)
ACT-CLJ0012.8–0855/J0012.9–0857	0.345	2.13	617	2924	2.50	1.91	8
ACT-CLJ1512.8+1418/J1512.8+1420	0.179	2.05	371	520	1.59	1.57	27

MUSTANG-2 compared to the work on the nearby A399-401 system.

3) Selection of ACT Cluster Pairs with Possible Intergalactic Filaments

From the most recent ACT cluster catalog (Hilton et al. 2021, Table 4), we selected close pairs of highly significant cluster detections in which both of the clusters had spectroscopic redshifts, where the redshift differences implied radial velocity differences $\Delta v_r < 3000$ km/s, the redshifts satisfied $z < 0.4$ (to reduce the X-ray exposures), declinations were $> -10^\circ$, and the pair had separations of $< 4'$. These last two criteria are to allow observations with MUSTANG-2. The two most significant pairs (strongest ACT SZ) are listed in Table 1, where the columns give the mean redshift, projected separation of the clusters (in arcmin and kpc), radial velocity difference, and masses of the two clusters within the radius r_{500} where the mean density is 500 times the critical density. Fig. 4 shows ACT y -parameter SZ images and DECaLS optical images of the two cluster pairs.

We also require higher spatial resolution X-ray data than provided by ROSAT. We have approved XMM observations of our two targets. The first cluster pair was observed recently, and we received the data just before this proposal was submitted. A crude first-look image is shown in Fig. 5. The second pair is a C target (not guaranteed, but likely given it is a fairly short X-ray exposure). Note that XMM has slightly better angular resolution than MUSTANG-2, and thus is an ideal compliment for our proposed observations.

4) Main Scientific Objectives:

• Detect and Characterize the Intergalactic Filament between the Two Clusters:

The MUSTANG-2 and ACT observations will be combined to determine the SZ y -parameter image on scales ranging from $10''$ to $5'$. The multiple frequency measurements in ACT allow dust foregrounds to be removed, and an SZ y -parameter map to be derived. The properties of filaments will be determined or limited by model fitting to the SZ y -images. Clusters will be modeled with elliptical radial profiles, which can be subtracted from the maps to reveal the filaments. The significance of filament detection will be measured by comparing the goodness of fits of models that simultaneously include a component for a filament to models that do not include such a component.

Our approved XMM X-ray observations will be analyzed using the same fitting technique to derive the properties of the filament. The techniques of combining the SZ and X-ray data developed for the A399-401 Bridge filament (H22) will be applied to each of these cluster pairs. Crudely, the X-ray image gives the integral of density squared, while the SZ image gives the integral of pressure. Combined with the X-ray temperature, this gives a density, and thickness of the filament, allowing its mass to be determined and compared to that of the two clusters and to the expected density of

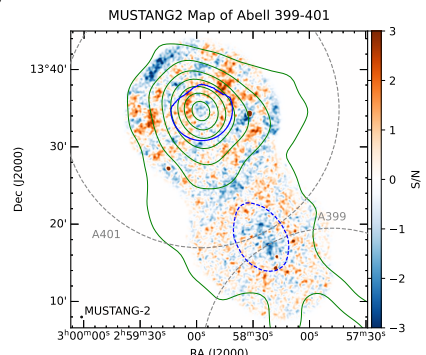


Fig. 3: MUSTANG-2 SZ image of Abell 401 and the upper portion of the A399-401 Bridge (H22). This high resolution image was used to search for fluctuations or shocks in the filament. The green contours are from Planck+ACT (Fig. 1). Note that A399 was not included and the bulk of the filament emission is resolved out by MUSTANG-2 due to the very low redshift.

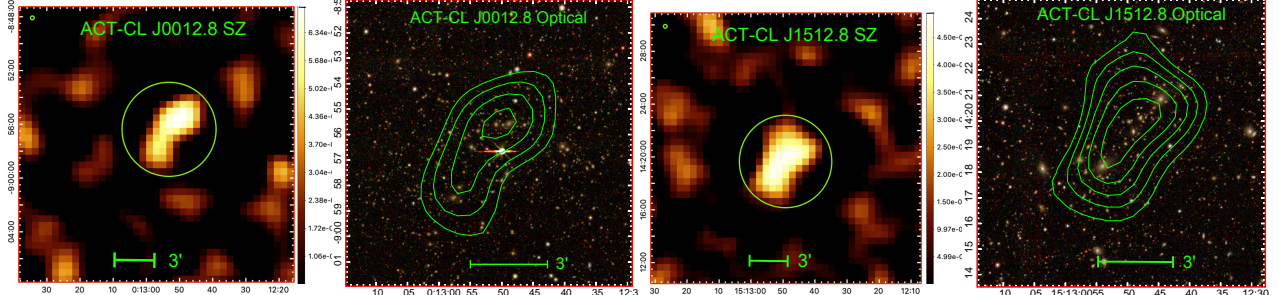


Fig. 4: For each of our two cluster pairs, the left image shows the ACT SZ Compton- y map (Hilton et al. 2021), while the DECALS zrg optical image (Dey et al. 2019) with ACT SZ contours is on the right. In the SZ images, the big circle is the $r = 3.5'$ scan pattern of MUSTANG-2, while the small circle at the upper left is the MUSTANG-2 resolution. The MUSTANG-2 images will extend $\sim 2'$ beyond the scan pattern due to the FOV of the instrument. The ACT SZ images show each cluster with a possible bridge between them.

baryons. The projected spatial separation and radial velocity difference can be used to model the overall geometry of the system, and correct for projection effects (as was done for A399-401).

- **Search for Intergalactic Shocks at the Sides of the Filaments:**

MUSTANG-2's very good angular resolution allows finer features to be detected. Shocks are expected at the edges of filaments of intergalactic gas where infalling gas hits the filament. These shocks are expected to be narrow, but with lengths comparable to the filament. Such a feature may have been seen in A399-401 with Suzaku (Fig. 2 above; Akamatsu et al. 2017). Of course, the approved XMM X-ray images can also allow these shocks to be detected. For both the SZ and X-ray, even if such a shock is too faint to be seen easily in the images, the surface brightness profiles perpendicular to the filament axis may show an SZ or X-ray emissivity jump.

- **Search for Merger Features in Each Cluster:**

Both the MUSTANG-2 SZ and X-ray images can show shocks within the individual clusters due to the cluster mergers. MUSTANG-2 images are particularly good at this as they image pressure directly. The XMM X-ray images can also see cold fronts and cool tails due to mergers. If seen, these will help to determine the dynamical state of the cluster pair. If the clusters are both regular with cool cores, it will indicate that these are still early pre-mergers.

- **Determine the Global Properties (e.g., Gas and Total Mass) of the Individual Clusters**

References: Akamatsu et al. 2017, A&A, 606, A1 • Bonjean et al., 2018, A&A, 609, A49 • Bouma et al., 2021, A&A, 647, A166 • Cen & Ostriker 1999, ApJ, 514, 1 • Dey, et al., 2019, AJ, 157, 168 (DECALS) • Fabian et al., 1997, MNRAS, 285, L35 • Fujita et al., 1996, PASJ, 48, 191 • Fujita et al., 2008, PASJ, 60, S343 • Fukugita et al., 1998, ApJ, 503, 518 • Hilton et al., 2021, ApJS, 253, 3H • Hincks, et al., 2022, MNRAS, 510, 3335 (H22) • Macquart, et al., 2020, Nature, 581, 391 • Markevitch et al., 1998, ApJ, 503, 77 • Mroczkowski et al., 2019, SSRev, 215, 17 • Planck Collaboration 2013, A&A, 550, A134 • Sakelliou & Ponman 2004, MNRAS, 351, 1439 • Schaan et al., 2021, PhysRevD, 103, 063513 • Tanimura et al., 2020a, A&A, 637, A41 • Tanimura et al., 2020b, A&A, 643, L2 • Tuominen et al., 2021, A&A, 646, A156

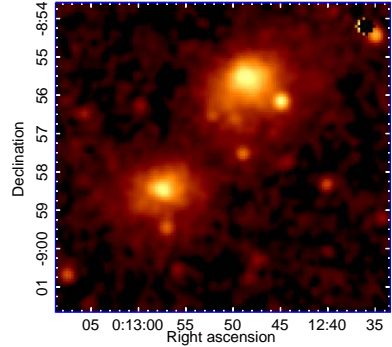


Fig. 5: Crude XMM X-ray image of our first cluster pair. (The data was received just before this proposal was submitted; the full analysis will yield a much deeper and cleaner image.) The image was corrected roughly for exposure and background, and smoothed to $10''$ resolution.